

Cast-Replicated NiTiCu Foams with Superelastic Properties

MARCUS L. YOUNG, JOHN D. DeFOUW, JAN FRENZEL, and DAVID C. DUNAND

Ni₄₀Ti₅₀Cu₁₀ foams were replication cast into a porous SrF₂ preform. This space holder is chemically stable in contact with liquid and solid Ni₄₀Ti₅₀Cu₁₀, but can be removed by dissolution in nitric acid. A Ni₄₀Ti₅₀Cu₁₀ foam with 60 pct porosity exhibits low stiffness (1 to 13 GPa) and large recoverable strains (~4 pct) during cyclical compression testing at 311 K (38 °C), within the superelastic range based on calorimetry results. This is the first time that replication casting is used to create an open foam of a NiTi-based shape-memory alloy, due to difficulties associated with the high reactivity and strong contamination tendency of the melt. Casting NiTi-based shape-memory alloy foams enable the economical production of porous actuators, energy absorbers, and biomedical implants with complex shapes.

DOI: 10.1007/s11661-011-1060-x

© The Minerals, Metals & Materials Society and ASM International 2012

I. INTRODUCTION

NEAR equiatomic NiTi (Nitinol) alloys exhibit a unique combination of properties: high static and cyclic strength, good ductility and toughness, low stiffness, excellent corrosion resistance, and unusual strain/shape recovery properties at ambient temperature based on the shape-memory effect or superelastic effect, depending on the exact Ni/Ti ratio. NiTi alloys are used in three main areas: (1) as biomedical implants because of their biocompatibility, low stiffness (as compared to other metals), higher radiopacity than titanium, and shape recovery (allowing *in-situ* deployment);^[1–3] (2) as actuators, using their shape-recovery properties;^[4–6] and (3) as high damping materials.^[7,8] Both the functional stability and hysteresis width of NiTi can be significantly improved by replacing some of the Ni with Cu,^[4] making ternary Ni_{50–x}Ti₅₀Cu_x alloys especially attractive for actuator applications. Adding porosity to NiTi-based alloys creates new functionality for these applications: (1) for implants, porosity reduces stiffness and the associated stress shielding, while allowing osseointegration; (2) for actuators, open porosity improves heat transfer by allowing fluid flow through the foam, and thus response time; and (3) for damping, porosity increases energy absorption by plastic collapse, and the open pores can also be filled with other damping materials, *e.g.*, elastomers.

As reviewed in References 9 through 12, nearly all processing methods developed to date for porous NiTi rely on powder metallurgy and are based on densifica-

tion of elemental or prealloyed powders. Pores are created by partial sintering of powders or by full densification followed by expansion of entrapped gas, or by removal of an entrapped solid space holder. However, densification of NiTi powders is often incomplete due to the poor sinterability of NiTi. This issue can be addressed by hot isostatic pressing (HIP) of prealloyed NiTi powders mixed with space holders,^[9,13] but the HIP method is slow and costly. Recently, we showed that the creation of a small quantity of a eutectic liquid, created *in situ* by reaction between NiTi and Nb powders or wires, fills the small space between the NiTi particles of the foam matrix without filling the larger pores created by the space holder.^[14,15] This method, however, results in a complex structure consisting of prior NiTi powders bonded by a NiTi-Nb eutectic phase. We are aware of only one case where porous NiTi was created in the liquid state: Sugiyama *et al.*^[16] subjected a NiTi rod to zone melting in a H₂/He mixture at 25 atm pressure: hydrogen dissolved in liquid NiTi upon melting and was then rejected during directional solidification, creating aligned, elongated pores.

While lower-melting metals are routinely foamed in the liquid state (*e.g.*, by gas injection or evolution in the melt^[17,18]), there are no reports on the production of porous NiTi using a liquid route to date, with the preceding exception. This is because NiTi has a high melting point (1583 K (1310 °C)) coupled with an extreme reactivity with residual gases and most ceramic materials^[7,8,19] and a high sensitivity to composition deviation: a small depletion (<0.1 at. pct) of the more reactive Ti significantly affects the transformation temperatures that control the shape-memory and superelastic effects.^[7,20] Recently, we demonstrated the use of high-melting space holders, which can be infiltrated with high-melting metallic melts: Zr alloys (with SrF₂ or BaF₂ as a space holder^[21]) and Ni alloys, (with NaAlO₂ as a space holder^[22,23]). This method has also been used for Ag alloys (with MgSO₄ as a space holder^[24]) and is well established for lower melting Al alloys (with NaCl as a space holder^[25]). The space holder must be insoluble and unreactive with the molten and solid alloy, while

MARCUS L. YOUNG, Alexander von Humboldt Fellow, and JAN FRENZEL, Head of the Research Group “Materials Processing and High Temperature Strength,” are with the Institut für Werkstoffe, Ruhr-Universität Bochum, Universitätsstraße 150, 44801 Bochum, Germany. JOHN D. DeFOUW, Postdoctoral Researcher, and DAVID C. DUNAND, James N. and Margie M. Krebs Professor, are with the Department of Materials Science and Engineering, Northwestern University, Evanston, IL 60208. Contact e-mail: myinfinitevision@gmail.com

Manuscript submitted May 19, 2011.

Article published online February 22, 2012

showing good solubility in a solvent or acid that does not attack the alloy. Halides of alkali- and alkaline earth metals (groups 1 and 2), which are soluble in water or acids, are particularly well suited as space holders for transition-metal alloys whose halides are much less stable.

Here, we demonstrate the use of SrF_2 as a space holder to create a replicated $\text{Ni}_{40}\text{Ti}_{50}\text{Cu}_{10}$ foam by the liquid route. We show that this foam, after solidification of the metal and removal of the space holder, exhibits thermal, mechanical, and shape-memory properties comparable to those of NiTi foams created by powder metallurgy. To our knowledge, this is the first time a NiTi-based foam was processed by liquid metal replication of a space-holder preform, thus opening the door to near-net-shape casting of porous NiTi and NiTi-based SMAs with complex shapes, for applications such as implants, actuators, and energy absorbers, in an economical manner.

II. EXPERIMENTAL PROCEDURES

As described in a previous study,^[21] SrF_2 powders with 180 to 355 μm size were packed into an Al_2O_3 crucible with inner and outer diameters of 19 and 25 mm, respectively, and sintered at 1673 K (1400 °C) for 10 hours under a vacuum with 10^{-4} Pa residual pressure. An Al_2O_3 spacer disc was placed on top of the partially densified SrF_2 preform, and a charge of $\text{Ni}_{40}\text{Ti}_{50}\text{Cu}_{10}$ alloy (referred to as NiTiCu in the following) was placed above the spacer in the alumina crucible. This composition was chosen because it is known to show small hysteresis widths,^[4,26] high intrinsic damping capabilities,^[27,28] and good functional stability;^[4] also, the transformation temperatures of this alloy are less strongly influenced than NiTi by the compositional changes that can easily occur during melting processes.^[29]

The NiTiCu alloy was then heated under high vacuum at 7 °C/min to 1375 °C (above its liquidus temperature^[30]) and held for 1 hour after which pressure was applied using Ar gas, bringing the furnace absolute pressure to 1 atm and forcing the NiTiCu melt into the porous SrF_2 preform. After furnace cooling, the resulting NiTiCu/ SrF_2 composite billet, illustrated in Figure 1, was sectioned into compression samples with approximate dimensions of $5 \times 10 \times 10 \text{ mm}^3$ using a low-speed diamond saw. These compression samples were subsequently ultrasonicated in a solution of 20 pct HNO_3 in distilled H_2O for 2 hours to remove the SrF_2 salt. To improve the shape-memory effect, the samples were last homogenized at 1173 K (900 °C) for 5 hours in evacuated quartz capsules, followed by water quenching.

Differential scanning calorimetry (DSC) was performed on the NiTiCu foam and on the original bulk alloy using a TA Instruments (New Castle, DE) DSC 2920CE instrument operating from -150 to 150 °C at a heating/cooling rate of 10 °C/min, with specimens held for 5 minutes at the maximum and minimum temperatures (Figures 2(a) and (b)). Further details of DSC testing are described elsewhere.^[31] Scanning electron

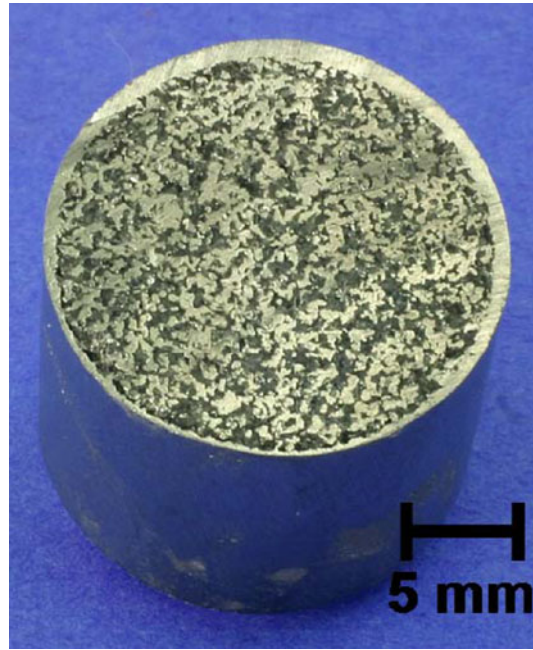


Fig. 1—Photograph of the NiTiCu/ SrF_2 composite prior to removal of the SrF_2 phase.

microscopy (SEM) with energy dispersive spectroscopy (EDX) was performed using a LEO 1530 VP instrument. Mass and volume measurements of the NiTiCu foam were used to calculate the total porosity, using 6.5 g/cm^3 as the density of bulk NiTiCu.^[32]

Compression testing was performed using a screw-driven load frame. Engineering strain was determined from crosshead motion corrected by the measured compliance of the system and calibrated by testing an aluminum sample with a known Young's modulus. The compression experiment was conducted at 311 K (38 °C) (body temperature), where the alloy is fully austenitic, with loading and unloading at a constant crosshead displacement rate of 0.05 mm/min over seven consecutive loops. Maximum strain for each loop was successively increased up to a maximum value of 6.9 pct, as shown in Table I. Average loading and unloading stiffness values, E_{load} and E_{unload} , were determined from the slope of a best linear fit from the linear portion of the loading and unloading curves, respectively (all compressive stresses and strains are reported as positive values in the present article).

III. RESULTS AND DISCUSSION

A. Microstructure

In addition to removal of the SrF_2 salt, Figures 3(a) and (b) show that a small amount of the NiTiCu matrix, as well as a secondary phase within it, are also removed during acid dissolution. Further inspection using SEM/EDX shows that the foam is composed of an austenitic (Ni,Cu)Ti matrix (bright phase in Figure 4(a)) and a $\text{Ti}_2(\text{Ni,Cu})$ secondary phase (dark phase in Figure 4(a)) that contains small amounts of oxygen. It is known that

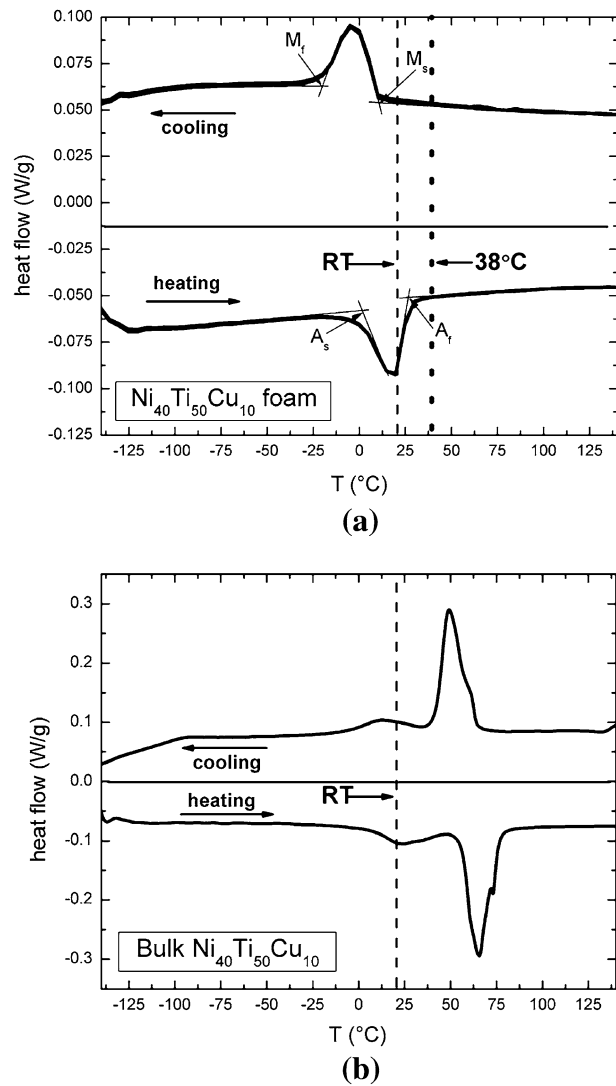


Fig. 2—(a) DSC curve of the heat-treated NiTiCu foam. The dashed line refers to room temperature, and the dotted line refers to the testing temperature 311 K (38 °C). (b) DSC curve of the cast, non-porous, bulk heat-treated NiTiCu material subsequently remelted to produce the NiTiCu foam.

Table I. Maximum Applied Strain, Stiffness on Loading and Unloading, Transformation Stress, and Irrecoverable Strain for the Superelastic NiTiCu Foam Subjected to Seven Compressive Load-Unload Loops at 311 K (38 °C)

ϵ_{\max} (Pct)	E_{load} (GPa)	E_{unload} (GPa)	σ_{Trans} (MPa)	ϵ_{irr} (Pct)
1.8	1.0	6.8	12.2	0
2.7	1.3	8.0	12.7	0
3.5	1.6	8.3	17.9	0
4.3	2.0	9.7	25.5	0.4
5.2	2.6	12.2	40.1	0.7
6.1	3.1	12.7	55.1	1.6
6.9	2.5	NA*	NA*	3.5

*NA: not applicable.

this phase corresponds to Ti_2Ni in binary NiTi, and that it can be stabilized by scavenging oxygen during the melting process.^[20] During solidification, a $\text{Ti}_2(\text{Ni,Cu})$ phase forms between NiTi cells/dendrites through a peritectic reaction.^[20,33] Ti_2Ni is known to be detrimental to the shape-memory effect because it promotes brittle fracture.^[34] Within the $\text{Ti}_2(\text{Ni,Cu})$ phase (dark phase in Figure 4(b)), SEM/EDX reveals three variants of corresponding $(\text{Ni,Cu})_4\text{Ti}_3$ precipitates (lighter lenticular disclike shapes, Figure 4(b)). The large lighter region in the upper right corner corresponds to a Cu-rich $(\text{Cu,Ni})_3\text{Ti}$ phase. These results show that not only does the acid remove the SrF_2 salt but it also selectively removes the predominant detrimental $\text{Ti}_2(\text{Ni,Cu})$ phase along with the two minor phases ($(\text{Ni,Cu})_4\text{Ti}_3$ precipitates and Cu-rich $(\text{Cu,Ni})_3\text{Ti}$ globules) within it.

The density of the sample was measured to be 2.71 g/cm³ corresponding to a relative density of 40.3 pct or a porosity of 59.7 pct. This relatively low value of density is likely due to good packing and partial sintering of SrF_2 powders and to some dissolution of the alloy matrix during leaching of the SrF_2 space holder, as shown with other foams.^[21,35] As with other salt replicated foams,^[9,13,14,21,22] the NiTiCu foam shown before salt removal in Figure 1 has the characteristically large node/strut length ratio due to the irregularly shaped and faceted salt space holder.

B. Transformation Behavior

The DSC curve of the NiTiCu foam after heat treatment and water quenching (Figure 2(a)) shows austenitic start ($A_s = 2.5$ °C) and finish ($A_f = 26.4$ °C) temperatures and martensitic start ($M_s = 9.4$ °C) and finish ($M_f = -18.9$ °C) temperatures, while the DSC curve of the bulk NiTiCu alloy (Figure 2(b)) shows two-step transformations with higher transformation temperatures. The DSC curve of the NiTiCu foam shows two noteworthy features: (1) the material exhibits one-step transformations on both cooling and heating, and (2) the start-temperature of the martensitic transformation on cooling is 9.4 °C. These two characteristics strongly differ from the behavior of dense bulk $\text{Ni}_{40}\text{Ti}_{50}\text{Cu}_{10}$ (Figure 2(b)), which shows two-step transformations on cooling (martensitic transformations of type B2 → B19 and B19 → B19') and heating (reverse transformation of type B19' → B19 and B19 → B2). Furthermore, bulk $\text{Ni}_{40}\text{Ti}_{50}\text{Cu}_{10}$ has a B19-start temperature of 333 K (60 °C),^[4] which is ~50 °C higher than in the porous material. These deviations can be explained by the formation of $\text{Ti}_2(\text{Ni,Cu})$ particles (Figure 4) during the production of the foam, which increases the Ni/Ti ratio of the alloy and thus depresses the phase transformation temperatures.^[20] It is likely that the formation of these phases can be reduced by an optimization of the processing conditions. For example, a reduction of holding time of the molten alloy and the use of calcium oxide crucibles might help reduce the level of oxygen contamination in the melt and, thus, reduce the formation of oxygen-stabilized $\text{Ti}_2(\text{Ni,Cu})$. The transformation enthalpies

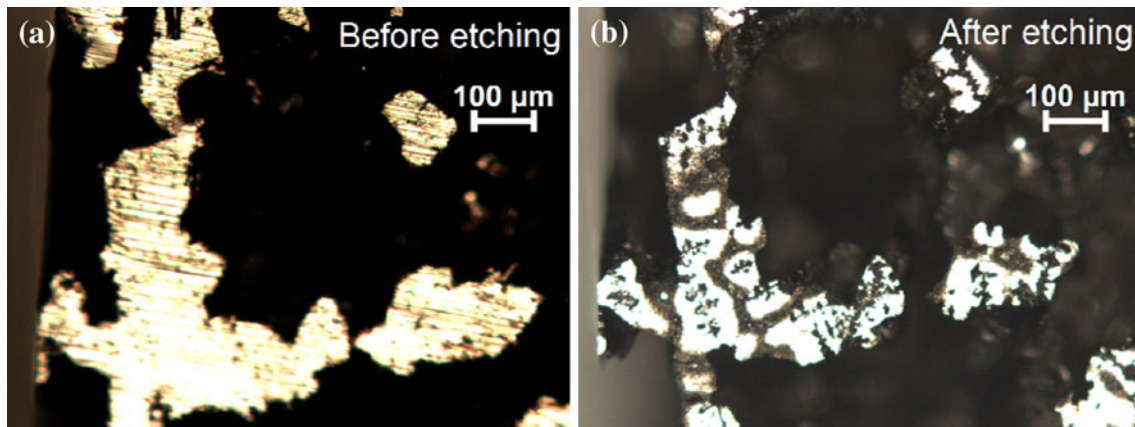


Fig. 3—Optical micrographs of a cross section of NiTiCu foam (a) before and (b) after acid exposure.

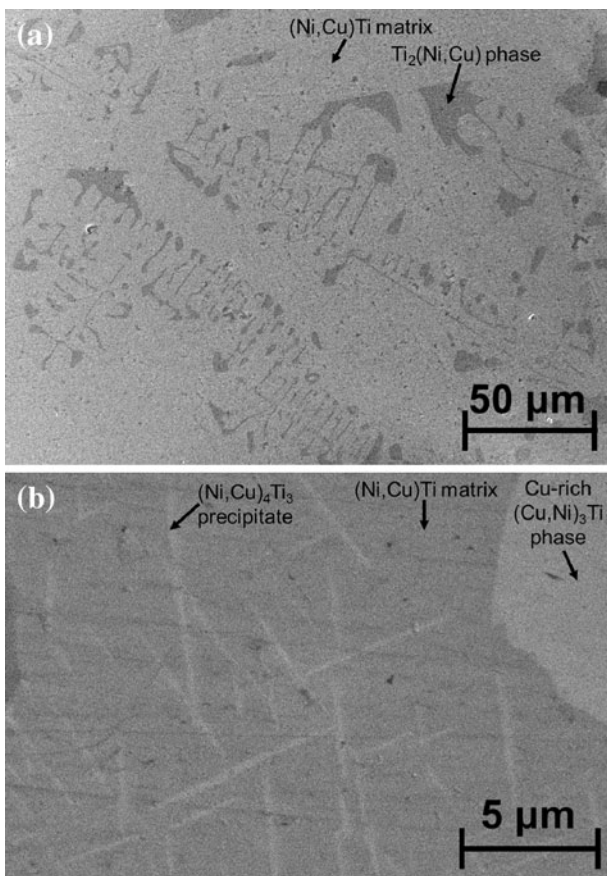


Fig. 4—Scanning electron microscope micrographs of the heat-treated NiTiCu foam before acid exposure. Arrows illustrate the various phases present.

(5.03 J/g upon cooling and -4.30 J/g upon heating) are relatively low as compared to bulk NiTiCu (cooling: B2 \rightarrow B19: 17 J/g, B19 \rightarrow B19': 2.7 J/g; heating: B19' \rightarrow B19: 3.2 J/g and B19 \rightarrow B2: 17 J/g) and to other similar NiTi foams;^[9,13,14,36,37] this is due to the additional phases present within the (Ni,Cu)Ti matrix, which affect the overall transformation response.

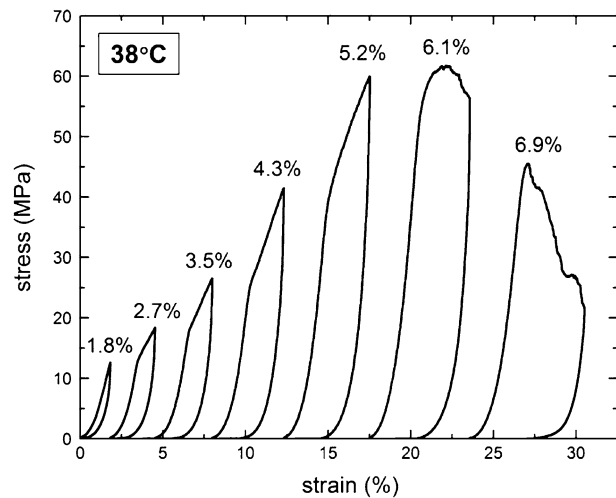


Fig. 5—Series of compressive stress-strain curves (load-unload) for the superelastic heat-treated NiTiCu foam subjected to increasing maximum strains at 311 K (38 °C). Curves are shifted along the x-axis for clarity.

C. Compressive Properties

Compressive load-unload stress-strain curves are shown in Figure 5 for the NiTiCu foam. All curves display on loading an initial elastic region (with some initial curvature probably due to slightly nonparallel faces of the sample in contact with the compression platens), which is associated with the elastic deformation of austenite. In the first loop (1.8 pct maximum strain), an inflection point is visible at a stress of ~ 11 MPa, which is expected to correspond to the onset of stress-induced martensite formation. Upon unloading, full recovery of the strain is observed, indicating that the reverse transformation has occurred. In the subsequent load-unload loop (2.7 pct maximum strain), a change in the slope of the stress-strain curve is observed once the maximum stress of the previous loop is obtained (in this case, 12.7 MPa). This behavior has a strong similarity to the occurrence of stress-strain plateaus with multiple stress levels observed for superelastic NiTi wires.^[38] In the first cycle, stress-induced martensite likely forms

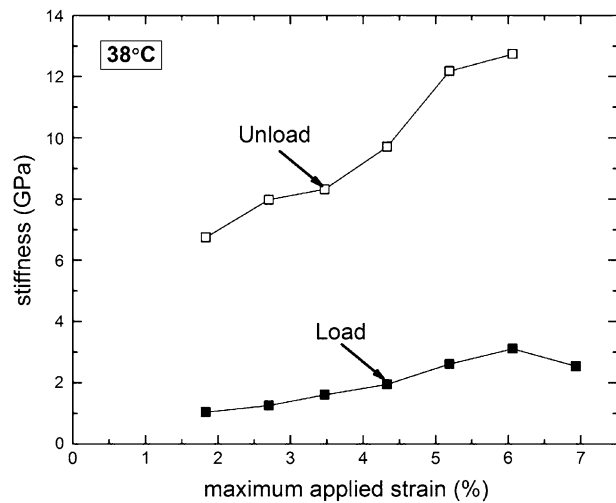


Fig. 6—Load and unload apparent stiffness as a function of maximum compressive strain for the superelastic heat-treated NiTiCu foam tested in compression at 311 K (38 °C).

locally in regions where the highest stresses occur (e.g., at the thinnest struts oriented such that the local stress is highest). The mechanical behavior evolves with each subsequent cycle due to irreversible effects as a result of dislocation accumulation, which in turn, stabilizes transformed martensite (i.e., retained martensite).^[38] Once the macroscopic load reaches a level that is higher than that in the previous cycle, the martensite grows into regions that were not previously transformed, leading to a change in the slope of the stress-strain curve; however, further experiments are required to test this hypothesis. This behavior of increasing transformation stress levels continues up to an applied strain of ~6 pct and ~60 MPa until the martensitic transformation appears complete, whereupon subsequent loading results in elasto-plastic deformation of martensite. This elasto-plastic deformation of martensite is expected to occur in the stress-strain curve shown in Figure 5 during the loop with 4.3 pct maximum strain, for which some irreversible strain (0.4 pct) appears for the first time after unloading; this can be interpreted as the presence of retained martensite stabilized by plastic strains, which constrain the reverse transformation. With the three subsequent loading cycles, the amount of irreversible strain increases: for the last two cycles with 6.1 and 6.9 pct maximum strain, damage of the NiTiCu foam occurs on loading (as visible from stress drops in Figure 5), resulting in significantly larger amounts of irreversible strain (1.6 and 3.5 pct, respectively) after unloading. In the final stress-strain curve (6.9 pct maximum strain), the sample can no longer support large stresses.

The Young's modulus E of the foam can be predicted by the Gibson-Ashby equation^[39]

$$E = (\rho^*)^2 E_{\text{NiTi}} \quad [1]$$

where ρ^* is the relative density (0.403 for the present NiTiCu foams) and E_{NiTi} is the Young's modulus for bulk NiTi (61 to 69 GPa^[40]). Equation [1] predicts values of 9.9 to 11.2 GPa, which are close to the

unloading foam stiffness values shown in Table I and Figure 6. As often observed in porous NiTi,^[9,13–15] the loading foam stiffness is much below the unloading value, which may be due to the early onset of super-elastic deformation during the nominally elastic part of the stress-strain curve on loading.

IV. CONCLUSIONS

Porous Ni₄₀Ti₅₀Cu₁₀ (NiTiCu) shape-memory alloys were created, for the first time, by a melt-infiltration technique, where SrF₂ was used as a space holder. The following key results were obtained.

1. The microstructure of the porous shape-memory alloy consists of austenitic (Ni, Cu)Ti and several secondary phases. Oxygen-stabilized Ti₂(Ni,Cu) was formed, most probably due to oxygen dissolved when the alloy was in the molten state. This phase was removed from the foam surface, together with the SrF₂ space holder, during acid exposure. A reduction in process duration and the replacement of aluminum oxide crucibles with calcium oxide crucibles might reduce the occurrence of this phase.
2. The transformation temperatures of the porous NiTiCu alloys are ~50 °C lower than usually found for cast, nonporous, bulk Ni₄₀Ti₅₀Cu₁₀. This shift in transformation temperatures is due to the formation of Ti₂(Ni,Cu), which increases the Ni/Ti ratio of the alloy.
3. A NiTiCu foam with ~60 pct porosity shows compressive load-unload curves characteristic of the superelastic effect—strains of up to ~4 pct recoverable on unloading and low stiffness values (1 to 3 GPa on loading, 7 to 13 GPa on unloading)—together with an ultimate compressive stress of ~60 MPa.

ACKNOWLEDGMENTS

The authors acknowledge funding by the Deutsche Forschungsgemeinschaft (DFG) through Subproject C7 of the Collaborative Research Center SFB 459 (with additional funding from the German state of North Rhine-Westphalia and Ruhr-Universität Bochum). MLY also acknowledges support by the Alexander von Humboldt Foundation.

REFERENCES

1. T. Duerig, A. Pelton, and D. Stockel: *Mater. Sci. Eng. A*, 1999, vols. 273–275, pp. 149–60.
2. N.B. Morgan: *Mater. Sci. Eng. A*, 2004, vol. 378 (1–2), pp. 16–23.
3. W. Cai, X.L. Meng, and L.C. Zhao: *Curr. Opin. Solid State Mater. Sci.*, 2005, vol. 9 (6), pp. 296–302.
4. C. Grossmann, J. Frenzel, V. Sampath, T. Depka, and G. Eggeler: *Metall. Mater. Trans. A*, 2009, vol. 40A, pp. 2530–44.
5. J. Frenzel, J.A. Burow, E.J. Payton, S. Rezanka, and G. Eggeler: *Adv. Eng. Mater.*, 2011, vol. 13 (4), pp. 256–68.
6. J. Van Humbeeck: *Mater. Sci. Eng. A*, 1999, vols. 273–275, pp. 134–48.

7. J. Frenzel, Z. Zhang, Ch. Somsen, K. Neuking, and G. Eggeler: *Acta Mater.*, 2007, vol. 55 (4), pp. 1331–41.
8. Z. Zhang, J. Frenzel, K. Neuking, and G. Eggeler: *Acta Mater.*, 2005, vol. 53 (14), pp. 3971–85.
9. A. Bansiddhi and D.C. Dunand: *Acta Biomater.*, 2008, vol. 4 (6), pp. 1996–2007.
10. S.A. Shabalovskaya: *Bio-Med. Mater. Eng.*, 2002, vol. 12, pp. 69–109.
11. G. Ryan, A. Pandit, and D.P. Apatisdhis: *Biomaterials*, 2006, vol. 27 (13), pp. 2651–70.
12. C.E. Wen, J.Y. Xiong, Y.C. Li, and P.D. Hodgson: *Phys. Scripta*, 2010, vol. T139, paper no. 014070, pp. 1–8.
13. A. Bansiddhi and D.C. Dunand: *Intermetallics*, 2007, vol. 15 (12), pp. 1612–22.
14. A. Bansiddhi and D.C. Dunand: *J. Mater. Res.*, 2009, vol. 24 (6), pp. 2107–17.
15. A. Bansiddhi and D.C. Dunand: *Adv. Eng. Mater.*, 2011, vol. 13 (4), pp. 301–05.
16. M. Sugiyama, S.K. Hyun, M. Tane, and H. Nakajima: *High Temp. Mater. Process.*, 2007, vol. 26, pp. 297–301.
17. L.P. Lefebvre, J. Banhart, and D.C. Dunand: *Adv. Eng. Mater.*, 2008, vol. 10 (9), pp. 775–87.
18. J. Banhart: *Adv. Eng. Mater.*, 2006, vol. 8 (9), pp. 781–94.
19. J. Frenzel, Z. Zhang, K. Neuking, and G. Eggeler: *J. Alloys Compd.*, 2004, vol. 385 (1–2), pp. 214–23.
20. J. Frenzel, E.P. George, A. Dlouhy, Ch. Somsen, M.F.X. Wagner, and G. Eggeler: *Acta Mater.*, 2010, vol. 58 (9), pp. 3444–58.
21. A.H. Brothers, R. Scheunemann, J.D. DeFouw, and D.C. Dunand: *Scripta Mater.*, 2005, vol. 52, pp. 335–39.
22. Y. Boonyongmaneerat and D.C. Dunand: *Adv. Eng. Mater.*, 2008, vol. 10 (4), pp. 379–83.
23. M. Chmielus, X.X. Zhang, C. Witherspoon, D.C. Dunand, and P. Müllner: *Nat. Mater.*, 2009, vol. 8 (11), pp. 863–66.
24. F. Diologent, E. Combaz, V. Laporte, R. Goodall, L. Weber, F. Duc, and A. Mortensen: *Scripta Mater.*, 2009, vol. 61 (4), pp. 351–54.
25. Y. Conde, J.F. Despois, R. Goodall, A. Marmottant, L. Salvo, C. San Marchi, and A. Mortensen: *Adv. Eng. Mater.*, 2006, vol. 8 (9), pp. 795–803.
26. R. Zarnetta, R. Takahashi, M.L. Young, A. Savan, Y. Furuya, S. Thienhaus, B. Maaß, M. Rahim, J. Frenzel, H. Brunken, Y.S. Chu, V. Srivastava, R.D. James, I. Takeuchi, G. Eggeler, and A. Ludwig: *Adv. Funct. Mater.*, 2010, vol. 20 (12), pp. 1917–23.
27. A. Biscarini, B. Coluzzi, G. Mazzolai, F.M. Mazzolai, and A. Tuissi: *J. Alloys Compd.*, 2003, vols. 356–357, pp. 669–72.
28. F.M. Mazzolai, A. Biscarini, B. Coluzzi, G. Mazzolai, E. Villa, and A. Tuissi: *Acta Mater.*, 2007, vol. 55 (13), pp. 4243–52.
29. O. Mercier and K. Melton: *Metall. Trans. A*, 1979, vol. 10A, pp. 387–89.
30. K.P. Gupta: *J. Phase Equilib.*, 2002, vol. 23 (6), pp. 541–47.
31. J. Khalil Allafi, X. Ren, and G. Eggeler: *Acta Mater.*, 2002, vol. 50 (4), pp. 793–803.
32. N. Frantz-Rodriguez, A. Bosseboeuf, E. Dufour-Gergam, V. Stambouli-Séné, G. Nouet, W. Seiler, and J.-L. Lebrun: *J. Micromech. Microeng.*, 2000, vol. 10 (2), p. 147.
33. R.W. Cahn: *Adv. Mater.*, 1991, vol. 3 (12), pp. 628–29.
34. J. Mentz, J. Frenzel, M.F.-X. Wagner, K. Neuking, G. Eggeler, H.P. Buchkremer, and D. Stoeber: *Mater. Sci. Eng. A*, 2008, vol. 491, pp. 270–78.
35. Y. Matsumoto, A.H. Brothers, S.R. Stock, and D.C. Dunand: *Mater. Sci. Eng. A*, 2007, vol. 447 (1–2), pp. 150–57.
36. A.J. Neurohr and D.C. Dunand: *Acta Biomater.*, 2011, vol. 7 (4), pp. 1862–72.
37. A.J. Neurohr and D.C. Dunand: *Acta Mater.*, 2011, vol. 59 (11), pp. 4616–30.
38. A. Yawny, M. Sade, and G. Eggeler: *Z. Metallkd.*, 2005, vol. 96, pp. 608–18.
39. L.J. Gibson and M.F. Ashby: *Cellular Solids: Structure and Properties*, Cambridge University Press, Cambridge, United Kingdom, 1997.
40. D. Dunand, D. Mari, M. Bourke, and J. Roberts: *Metall. Mater. Trans. A*, 1996, vol. 27A, pp. 2820–36.